Table S1. List of 72 predictor variables assembled for fitting the ecological niche models of *Ivesia webberi*. They were reduced to 6 uncorrelated ($r > 0.6$) predictors using Kendall *r* correlation, and feature selection runs in *Boruta* R package and recursive feature elimination algorithm in *caret* R package.

Predictor name	**Description and source**
Elevation	A 30 m (1 arc second) digital elevation model (DEM) from National elevation dataset (USGS 2017)
Slope	Slope was calculated from the USGS (2017) DEM, using the slope tool in ArcMap version 10.7
Curvature	Curvature was calculated from the USGS (2017) DEM, using the slope tool in ArcMap version 10.7
Land cover	Sourced from the 30 m U.S. National Land Cover Dataset (NLCD) 2011 product (Homer et al. 2015)
Sine aspect	Sine aspect was calculated in ArcMap version 10.6.1 using USGS (2017) DEM and the slope
Cosine aspect	Cosine aspect was calculated in ArcMap version 10.6.1 using USGS (2017) DEM and the slope, the formula: $\theta \times \cos(\alpha)$, where = θ is slope (in percentage), and α is aspect (in radians)
Cosine aspect at 45°	Cosine aspect was calculated in ArcMap version 10.6.1 using USGS (2017) DEM and the slope, the formula: = $\theta \times \cos(\alpha)$, where = θ is slope (in percentage), and α is aspect (in radians). Here, aspect is tilted at 45° toward the southwest
Hillshade	A topographic variable calculated from the USGS (2017) DEM, using the hillshade tool in ArcMap version 10.6.1
Topographic Position Index (TPI33)	Calculated from USGS (2017) DEM in ArcMap version 10.6.1, using formula introduced by Weiss (2001), and a 33 m neighborhood
Topographic Position Index (TPI333)	Calculated from USGS (2017) DEM in ArcMap version 10.6.1, using formula introduced by Weiss (2001), and a 333 m neighborhood. At 333 m scale, the landscape is classified into either a valley or a mountain range
Topographic Wetness Index	Calculated from USGS (2017) DEM following the formula of Beven & Kirkby (1979) and is defined using the following formula: ln(upslope area/tan(slope)).
Annual herbaceous cover	Data was sourced from the Multi-Resolution Land Characteristics (MRLC) development of the U.S. National Land Cover Database (NLCD) 2016 Shrub component products (Xian et al. 2013)
Bare ground	
Artemisia tridentata cover	
Perennial herbaceous cover	
Soil litter	
Artemisia spp. cover	
Shrub vegetative cover	
Shrub height	
Sagebrush height	
Forest cover	A 30 m vegetative cover developed by the United States Forest Service (USFS) from multispectral LANDSAT imagery (Coulston et al. 2012)
Modified soil-adjusted vegetation index (MSAVI2)	Vegetation indices were created in Google Earth Engine, using remotely sensed data between January 1985 and December 2010, from LANDSAT 5, 7 and 8 images, using code developed by Brehm & Matos (2019)
Normalized difference vegetation index (NDVI)	

Solar radiation	Solar radiation was calculated in ArcMap using hemispherical viewshed algorithm (Fu & Rich, 2002) on the USGS (2017) DEM, in ArcMap version 10.6.1. Solar radiation was calculated for one day each in the four seasons: Julian days 1, 90, 225 and 287 for winter, spring, summer and fall respectively (except for leap years where Julian days 91, 226 and 288 represent spring, summer and fall respectively). Five-year interval area solar radiation was calculated between 1975 and 2018.
Available water content (AWC)	Edaphic variables sourced from POLARIS, a 30 m probabilistic soil series map of the United States (Chaney et al. 2016)
Soil mean $CaCO_3$	
Soil mean clay	
Soil mean silt	
Soil mean sand	
Soil mean pH	
Soil mean bulk density	
Soil organic matter	
Depth to restrictive layer (bedrock)	
Soil class	A gridded soil survey geographic (gSSURGO) from the United States, developed by the USDA Natural Resources Conservation Service (Soil Survey Staff 2017)
Geology	Environmental variable obtained from the Geologic maps of U.S. states (Horton et al. 2017) at https://mrdata.usgs.gov/geology/state
Cumulative annual actual evapo-transpiration (AET)	Water balance variable calculated from 800 m 1971-2000 PRISM climate normals (Daly et al. 2008), available water capacity (Chaney et al. 2016), and the 1-arcsecond DEM (USGS, 2017) combined in the Climatic Water Deficit Toolbox for ArcGIS (Dilts 2014). Methods are described in Dilts et al. (2015). AET represents the simultaneous availability of water and energy to support plant productivity.
Cumulative annual climatic water deficit (CWD)	Water balance variable calculated from 800 m 1971-2000 PRISM climate normals (Daly et al. 2008), available water capacity (Chaney et al. 2016), and the 1-arcsecond DEM (USGS, 2017) combined in the Climatic Water Deficit Toolbox for ArcGIS (Dilts 2014). Methods are described in Dilts et al. (2015). CWD is a measure of aridity and is difference between evaporative demand and supply
Cumulative annual potential evapo-transpiration (PET)	Water balance variable calculated from 800 m 1971-2000 PRISM climate normals (Daly et al. 2008), available water capacity (Chaney et al. 2016), and the 1-arcsecond DEM (USGS 2017) combined in the Climatic Water Deficit Toolbox for ArcGIS (Dilts 2014). Methods are described in Dilts et al. (2015). PET was calculated using the Thornthwaite approach outlined in Lutz et al. (2010).
Cumulative annual soil water balance (SWB)	Water balance variable calculated from 800 m 1971-2000 PRISM climate normals (Daly et al. 2008), available water capacity (Chaney et al. 2016), and the 1-arcsecond DEM (USGS 2017) combined in the Climatic Water Deficit Toolbox for ArcGIS (Dilts 2014). Methods are described in Dilts et al. (2015). SWB represents the amount of soil water storage summed across all months of the year.
Absolute cumulative soil water balance	Absolute value of the SWB. Calculated using 800 m resolution PRISM climatic data 1970-2001 normals (Daly et al. 2008), in BIOLCLIM (Booth et al. 2014)

Cumulative annual water supply (WS)	Water balance variable calculated from 800 m 1971-2000 PRISM climate normals (Daly et al. 2008), available water capacity (Chaney et al. 2016), and the 1-arcsecond DEM (USGS 2017) combined in the Climatic Water Deficit Toolbox for ArcGIS (Dilts 2014). Methods are described in Dilts et al. (2015). WS is the sum of rainfall and snowmelt in all months
Monsoonality	Proportion of annual precipitation falling between July and September (Romme et al. 2009). Original data source from 800 m resolution PRISM climatic data normals 1971-2000 (Daly et al. 2008)
Heatload	Static measure of solar radiation exposure based on slope, aspect, and latitude, based on methods published in McCune & Keon (2002). DEM derivatives were based on the 1-arcsecond National Elevation Dataset (USGS 2017).
Minimum monthly temperature	Based on the 800 m PRISM climatic data normals 1971-2000 (Daly et al. 2008)
Maximum monthly temperature 1970-2001	
Minimum annual temperature	
Minimum spring temperature	
Minimum fall temperature	
Minimum summer temperature	
Minimum winter temperature	
Maximum spring temperature	
Maximum summer temperature	
Maximum fall temperature	
Maximum winter temperature	
Annual monthly precipitation	
Fall seasonal precipitation	
Spring seasonal precipitation	
Summer seasonal precipitation	
Winter seasonal precipitation	
Temperature range	
Ratio of AET and CWD	Water balance variables calculated from 4 km 1950-2015 PRISM climate monthly data (Daly et al. 2008), available water capacity (Chaney et al. 2016), and the 1-arcsecond DEM (USGS 2017) combined in the Climatic Water Deficit Toolbox for ArcGIS (Dilts 2014). PRISM climate data were downscaled to 800 m using the delta method and the PRISM 1971-2000 normals. Variables are described in Barga et al. (2018).
Ratio of AET and PET	
Ratio of SWB and AET	
Ratio of WS and AET	
Positive difference between AET and SWB	
Absolute ratio of SWB and AET	

Spring ratio of WS and the greater of AET or SWB	
Precipitation seasonality	Based on PRISM climatic data normals 1971-2000 (Daly et al. 2008), in BIOCLIM (Booth et al. 2014).
April snowpack (1951 – 1980)	Water balance variables calculated from 4 km 1950-2015 PRISM climate monthly data (Daly et al. 2008), available water capacity (Chaney et al. 2016), and the 1-arcsecond DEM (USGS 2017) combined in the Climatic Water Deficit Toolbox for ArcGIS (Dilts 2014). PRISM climate data were downscaled to 800 m using the delta method and the PRISM 1971-2000 normals. Variables are described in Barga et al. (2018).
April snowpack (1981 – 2010)	
Recharge 1951-1980	
Recharge 1981-2010	

Table S2. Overview, data, model, assessment and prediction (ODMAP) reporting protocol describing the main steps in building the iterative niche modeling for *Ivesia webberi* in the western Great Basin Desert

ODMAP element	**Contents**
OVERVIEW	
Authorship	**Authors**: Israel T. Borokini, Kenneth Nussear, Blaise Petitpierre, Thomas E. Dilts, Peter J. Weisberg **Contact email**: iborokini@berkeley.edu **Title**: Iterative ecological niche modeling results in the discovery of novel populations of a rare cold desert perennial DOI: 10.3354/esr01218
Model objective	**SDM objective**: mapping/interpolation **Target output**: continuous habitat suitability (probability of species occurrence)
Taxon	*Ivesia webberi*, a federally threatened forb in the Great Basin Desert, western Nevada
Location	Western Great Basin Desert and the eastern foothills of the Northern Sierra Nevada range
Scale of analysis	**Spatial extent (Long/Lat)**: 40.55 – 38.23N, -120.18 - -119.51W **Spatial resolution**: 30 m **Temporal extent**: period of climate normal (30 prior years averaged) **Temporal resolution**: single time period **Boundary**: spatial extent buffered by 60 km
Biodiversity data overview	**Observation type**: field survey **Response data type**: presence/true absence
Type of predictors	Bioclimatic, topographic, biotic, edaphic, land/vegetative cover
Conceptual model/hypothesis	Hypothesis: Bioclimatic, topographic and vegetation cover are important drivers of *Ivesia webberi* niche and distribution
Assumptions	1. Species are at equilibrium with their environment. 2. Important ecological drivers or their proxies of *Ivesia webberi* distributions are included
SDM algorithms	**Modeling algorithms**: Generalized linear models (GLM), Generalized additive models (GAM), Boosted Regression Trees (BRT), Random Forests (RF), Maximum Entropy (MAXENT), and Artificial Neural Networks (ANN) **Model complexity**: We used default parameter tuning in BRT, GLM, GAM, RF and ANN. For MAXENT, we used only linear and quadratic functions. **Model averaging/ensemble modeling**: Model averaging of 10 replicates for each of the six model algorithms, and weighted ensemble modeling. In addition, preliminary niche models were conducted to quantify the effect of uncertainties introduced in the SDM analysis steps. We tested the effect of biomod2 parameter tuning such as the prevalence function and the size of the cross-validation data.
Model workflow	• A total of 72 predictor variables were assembled and subjected to three consecutive variable selection analyses (Kendall correlation coefficient, caret recursive

	feature elimination, and Boruta variable reduction) from which six uncorrelated predictor variables were selected. • Preliminary niche models were fitted and the best three variables (from jackknife analysis of variable importance) were selected for the final niche models • Niche models were fitted in 2015, 2018, 2019 and 2020, hereafter called iterative niche models. Following each iterative niche model, field surveys were conducted in the predicted suitable sites. • Separate niche models with data partitioning via spatial blocking were also fitted • Spatial data (new occurrence and true absence points) collected from these field surveys were added to existing data for further iterative niche models, until the final field surveys in 2020, followed by the final iterative niche model • In all preliminary and iterative niche models, model performance was evaluated using 10-fold cross validation • Environmental conditions in original spatial data were compared with those of the new spatial data from field surveys using PCA-based niche overlap analysis
Software	**Software**: R (versions 4.0 – 4.2) with packages biomod2, dismo, mgcv, nnet, gbm, gam, MASS, randomForest (niche modeling), sp, raster, rgeos, rgdal, reshape (geospatial processing), Boruta, caret, stats (predictor variable reduction and selection), gplot (model plots), spThin (thinning of absence points), blockCV (spatial blocking of dataset), ecospat (niche differentiation), FNN (estimation of distance between points) **Code availability**: available on request **Data availability**: presence data available on request to the U.S. Fish and Wildlife Service
DATA	
Biodiversity data	**Taxon name**: *Ivesia webberi* **Taxon reference system**: Flora of North America **Ecological level**: species **Data sources**: Initial data was sourced from U.S. Fish and Wildlife Service (USFWS), Nevada Natural Heritage Program (NNHP), and augmented with model-guided field surveys **Sampling design**: Opportunistic detection during past vegetative surveys, surveys during environmental impact assessment of projects, model-guided field surveys **Sampling size**: 23 (as of 2015), and 32 (in 2020) Clipping: Spatial extent of *Ivesia webberi* occurrence buffered by 60 km **Absence data**: archived field surveys by NNHP botanists where *I. webberi* is confirmed absent, additional absence data were included from model-guided field surveys **Potential error and biases**: biased historical sampling, detection is optimized during the flowering season of the species (May-June), therefore false non-detection (false absence) may have occurred in previous vegetative surveys
Data partitioning	**Selection of training data**: 10-fold cross validation **Selection of truly independent test data**: given a small number of occurrence points, data partitioning into independent training and test data was not done
Predictor variables	**Predictor variables**: We assembled 72 predictor variables based on the understanding of the species, availability of data, and from field experts' advice. Bioclimatic variables: seasonal mean and annual minimum and maximum temperature, seasonal mean and annual minimum and maximum precipitation, solar radiation, heatload, cumulative annual actual evapo-transpiration (AET), cumulative annual potential evapo-transpiration (PET), cumulative climatic water deficit (CWD), available water content, cumulative annual soil water balance (SWB), cumulative annual water supply (AWS), monsoonality, precipitation seasonality, temperature range, April snowpack (1951 – 1980), April snowpack (1980 – 2010), recharge (1951-1980), recharge (1981-2010), absolute SWB, ratio of AET and CWD, ratio of AET and PET, ratio of SWB and AET, ratio of water supply and AET, positive difference between AET

	and SWB, absolute ratio of SWB and AET, spring ratio of WS and the greater of AET or SWB Topographic variables: cosine aspect, cosine aspect at 45°, topographic position index at 33 m, and at 333 m, Topographic Wetness Index, sine aspect, slope, elevation, hillshade, curvature, Edaphic variables: soil classes, soil mean $CaCO_3$, soil mean clay, soil mean silt, soil mean sand, soil mean pH, geology, bare ground, soil litter, soil mean bulk density, depth to bedrock, organic matter Cover: land cover Biotic variables: average modified soil-adjusted vegetation index (MSAVI2), average normalized difference vegetation index (NDVI), forest cover, annual herbaceous vegetative cover, *Artemisia tridentata* cover, perennial herbaceous cover, *Artemisia* spp. cover, shrub cover, shrub height, sagebrush height **Data sources and processing**: see Table S1 for a list of the predictors and their sources. **Spatial resolution of raw data**: Original PRISM climatic data from which the bioclimatic variables were developed were in 4 km. **Projection**: UTM
MODEL	
Variable pre-selection	Topographic variables were included based on literature the contribution of topographic variables to species endemism in the Great Basin Desert. Bioclimatic variables have been established as an important driver of species distribution at various spatial scales. Biotic variables were included because of the Eltonian noise hypothesis indicating the importance of biotic interactions on the distribution of species in fine scales (de Araújo et al. 2014). Moreover, studies have shown that plant species engage in ecological facilitation under abiotic stress such as the heat in the Great Basin Desert
Multicollinearity	Three variable reduction analyses were conducted. First, a number of correlated variables ($r \geq 0.6$) were removed using Kendall correlation coefficient, followed by recursive feature elimination (RFE) algorithm in caret R package, and Boruta algorithm in Boruta R package. Additional AIC-based stepwise model selection was done using the model performance metrics from the different preliminary niche models.
Model setting	GLMs were generated using quadratic terms in stepwise approach and using the Akaike information Criterion (AIC) for model selection. BRT models were generated by fitting 2500 trees and three cross-validations, while GAMs were analyzed with a spline smoothing function. We used five cross-validations to select the optimal hidden layers in ANN models, we fitted 500 random forest models, and ran MAXENT models with 10,000 background points, using linear, quadratic and product features but with logistic model output
Model estimates	**Uncertainty in model coefficients**: cross-validation was used to optimize model performance. **Variable importance**: quantification of deviance each variable explains, based on the ensemble models
Non-independence	**Method for addressing spatial autocorrelation**: As explained in literature, spatial clumping of occurrence points may not necessarily indicate spatial autocorrelation, but an indication of dispersal limitation and biotic interactions that limit spread. Given that the clumping in the data occurs near the center of the species range, the spatial distribution of *Ivesia webberi* may follow the predictions of the abundant-center hypothesis. Moreover, the machine learning algorithms used (e.g., BRT and RF) are robust to spatially autocorrelated data. Therefore, we did not check the model residuals for spatial dependence.
Threshold	Threshold that minimizes omission error was selected since the study species has fewer occurrence.
ASSESSMENT	
Performance statistics	**Model performance**: Model performance was assessed on the cross-validated data using a) specificity, a measure of omission errors, b) true skill statistic, a threshold-based

	metric of overall accuracy, c) area under curve (AUC) of the receiver operating characteristic, a threshold-independent plot of sensitivity values vs specificity values, and d) Boyce index, a Spearman's rank correlation of model predictions and the occurrence points. Statistical difference in the model performance metrics across years was also assessed. Multivariate multiple linear regression was used to test statistical difference in the scores of the four model performance metrics for each of the 10 model replicates of the six algorithms. **Model overfitting:** We used spatial blocking method to assess overfitting of the iterative niche models. Blocking is a nonrandom allocation of spatial data to reduce the effect of spatial bias and autocorrelation in the resulting models (Valavi et al. 2019). The same spatial dataset used for the iterative niche modeling each year were partitioned into three spatial blocks, two of which were used for training while the third block was used for testing. The three spatial blocks resulted from an initial partitioning of the entire study area into six latitudinal and longitudinal bins. Due to data requirement by different algorithms, we limited the niche modeling to Random Forest, Maximum Entropy, and Artificial Neural Networks. Overfitting was assessed as a difference between the training and test AUC (Warren & Seifert 2011).
Plausibility check	**Response plots**: Species-environment relationships were illustrated in response curves for each of the six algorithms
PREDICTION	
Prediction output	**Prediction unit**: suitable and non-suitable **Model projections**: Projections were limited to the study area and current time, no extrapolation to new space or time. Predictions of habitat suitability was done using weighted ensembles of the single model algorithms that have TSS $\geq$ 0.7. Prediction uncertainty maps were also produced. Map projections were made in ArcMap version 10.7 **Algorithm uncertainty**: six algorithms used, and ensemble modeling **Post-prediction**: Predicted suitable sites from each iterative niche models were visited between May and June of 2015, 2016, 2017, 2018 and 2019. This resulted in the discovery of seven new locations of the species. Coordinates of the predicted suitable sites where the species was not located were used as additional absence points.

Table S3. The relationship between the environmental variables and the first two axes of the principal component analysis based on the *Ivesia webberi* presence and true absence points

Environmental variables	PC1 (28.7%)	PC2 (20.3%)	PC3 (17.4%)
Actual evapotranspiration	-0.154	-0.607	0.600
Cosine aspect	0.159	0.791	0.033
Perennial herbaceous cover	0.015	0.436	0.776
Summer seasonal precipitation	0.868	-0.122	0.087
Minimum monthly temperature	-0.742	0.121	0.173
Topographic Position Index	0.605	-0.051	0.212

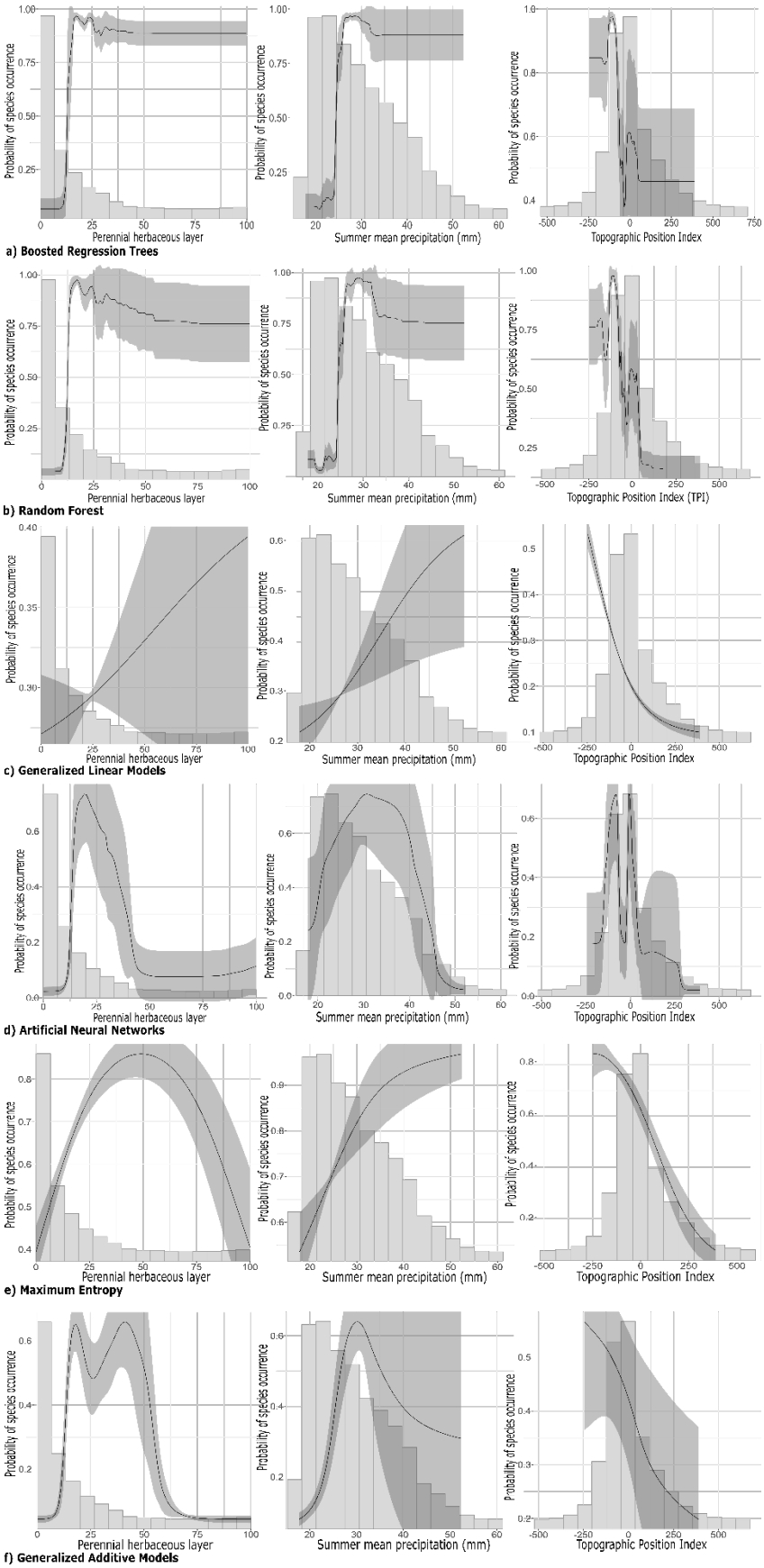

Fig. S1. Partial response plots showing the predicted probability of *Ivesia webberi* occurrence for the three predictor variables in the 2020 species distribution modeling iterations across the six algorithms. On each graph, the curves represent each of the 10 model replicates. The black line represents the average response for the 10 modeling replicates, while the grey shading surrounding it represent standard deviation

References

Barga SC, Dilts TE, Leger EA (2018) Contrasting climate niches among co-occurring subdominant forbs of the sagebrush steppe. Divers Distrib 24:1291–1307. doi:10.1111/ddi.12764

Beven KJ, Kirkby MJ (1979) A physically based, variable contributing area model of basin hydrology. Hydrol Sci J 24:43–69. doi:10.1080/02626667909491834

Booth TH, Nix HA, Busby JR, Hutchinson MF (2014) BIOCLIM: the first species distribution modelling package, its early applications and relevance to most current MaxEnt studies. Divers Distrib 20:1–9. doi:10.1111/ddi.12144

Brehm J, Matos A (2019) Google Earth Engine Landsat Compositor Javascript code for Google Earth Engine. University of Nevada Reno. Available at: https://code.earthengine.google.com/a86bca4669160b79b3bb60eec08556cc

Chaney NW, Wood EF, McBratney AB, Hempel JW, Nauman TW, Brungard CW, Odgers NP (2016) POLARIS: A 30-meter probabilistic soil series map of the contiguous United States. Geoderma 274:54–67. doi:10.1016/j.geoderma.2016.03.025

Coulston JW, Moisen GG, Wilson BT, Finco MV, Cohen WB, Brewer CK (2012) Modeling percent tree canopy cover: a pilot study. Photogramm Eng Remote Sensing 78:715–727. doi:10.14358/PERS.78.7.715

Daly C, Halbleib M, Smith JI, Gibson WP and others (2008) Physiographically-sensitive mapping of temperature and precipitation across the conterminous United States. Int J Climatol 28:2031–2064. doi:10.1002/joc.1688

Dilts TE (2014) Climatic Water Deficit Toolbox for ArcGIS 10.1. University of Nevada Reno. Available at: https://www.researchgate.net/publication/263083292_Climatic_Water_Deficit_Toolbox_for_ArcGIS_101

Dilts TE, Weisberg PJ, Dencker CM, Chambers JC (2015) Functionally relevant climate variables for arid lands: a climatic water deficit approach for modelling desert shrub distributions. J Biogeogr 42:1986–1997. https://doi.org/10.1111/jbi.12561

Fu P, Rich PM (2002) A geometric solar radiation model with applications in agriculture and forestry. Comput Electron Agric 37:25–35. doi:10.1016/S0168-1699(02)00115-1

Homer CG, Dewitz JA, Yang L, Jin S and others (2015) Completion of the 2011 National Land Cover Database for the conterminous United States-Representing a decade of land cover change information. Photogramm Eng Remote Sensing 81:345–354. doi:10.14358/PERS.81.5.345

Horton JD, San Juan CA, Stoeser DB (2017) The State Geologic Map Compilation (SGMC) geodatabase of the conterminous United States (ver. 1.1, August 2017). US Geol Surv Data Ser 1052. https://doi.org/10.3133/ds1052

Lutz JA, Van Wagtendonk JW, Franklin JF (2010) Climatic water deficit, tree species ranges, and climate change in Yosemite National Park. J Biogeogr 37:936–950. doi:10.1111/j.1365-2699.2009.02268.x

McCune B, Keon D (2002) Equations for potential annual direct incident radiation and heat load. J Veg Sci 13:603–606. doi:10.1111/j.1654-1103.2002.tb02087.x

Romme WH, Allen CD, Bailey JD, Baker WL and others (2009) Historical and modern disturbance regimes, stand structures, and landscape dynamics in pinon–juniper vegetation of the western United States. Rangeland Ecol Manag 62:203–222. doi:10.2111/08-188R1.1

Soil Survey Staff (2017) Gridded Soil Survey Geographic (gSSURGO) Database for the United States of America and the Territories, Commonwealths, and Island Nations served by the USDA-NRCS. United States Department of Agriculture, Natural Resources Conservation Service. Available online at http://datagateway.nrcs.usda.gov/. January 2017

U.S. Geological Survey [USGS] (2017) 1 Arc-second Digital Elevation Models (DEMs) - USGS National Map 3DEP Downloadable Data Collection. U.S. Geological Survey. Accessed at https://www.usgs.gov/core-science-systems/ngp/tnm-delivery/

Valavi R, Elith J, Lahoz-Monfort JJ, Guillera-Arroita G (2019) blockCV: an R package for generating spatially or environmentally separated folds for k-fold cross-validation of species distribution models. Methods Ecol Evol 10:225–232. doi:10.1111/2041-210X.13107

Warren DL, Seifert SN (2011) Ecological niche modeling in Maxent: the importance of model complexity and the performance of model selection criteria. Ecol Appl 21:335–342. doi:10.1890/10-1171.1

Weiss A (2001) Topographic position and landform analysis. Poster presentation, ESRI User Conference, San Diego, California, USA

Xian G, Homer C, Meyer D, Granneman B (2013) An approach for characterizing the distribution of shrubland ecosystem components as continuous fields as part of NLCD. ISPRS J Photogramm Remote Sens 86:136–149. doi:10.1016/j.isprsjprs.2013.09.009